



## OPEN ACCESS

## EDITED BY

Jie Fu,  
Chongqing University, China

## REVIEWED BY

Song Qi,  
Chongqing University, China  
Bochao Wang,  
University of Science and Technology of  
China, China

## \*CORRESPONDENCE

Chenguang Niu,  
✉ niuchenguang@tyut.edu.cn

RECEIVED 01 November 2023

ACCEPTED 06 December 2023

PUBLISHED 18 December 2023

## CITATION

Ti G, Fan Y, Tang J, Niu C and Xiong X  
(2023), Preparation and enhanced  
electrorheological properties of  
elastomers filled with rod-shaped  
TiO<sub>2</sub> particles.  
*Front. Mater.* 10:1331513.  
doi: 10.3389/fmats.2023.1331513

## COPYRIGHT

© 2023 Ti, Fan, Tang, Niu and Xiong. This  
is an open-access article distributed  
under the terms of the [Creative  
Commons Attribution License \(CC BY\)](#).  
The use, distribution or reproduction in  
other forums is permitted, provided the  
original author(s) and the copyright  
owner(s) are credited and that the original  
publication in this journal is cited, in  
accordance with accepted academic  
practice. No use, distribution or  
reproduction is permitted which does not  
comply with these terms.

# Preparation and enhanced electrorheological properties of elastomers filled with rod-shaped TiO<sub>2</sub> particles

Gang Ti<sup>1,2</sup>, Yi Fan<sup>2</sup>, Jian Tang<sup>2</sup>, Chenguang Niu<sup>2\*</sup> and Xiaoyan Xiong<sup>2</sup>

<sup>1</sup>Shanxi Bethune Hospital, Shanxi Academy of Medical Sciences, Taiyuan, China, <sup>2</sup>College of Mechanical and Vehicle Engineering, Taiyuan University of Technology, Taiyuan, China

The morphology of dispersed particles has been proven to have a significant impact on performance of electrorheological (ER) materials, while there is a lack of relevant research on its impact on the properties of electrorheological elastomers (EREs). In this study, the TiO<sub>2</sub> particles with spherical, short rod, and long rod shape were fabricated with sol-gel method, and the EREs were prepared with these three kinds of particles as dispersion phase. Particle characterization results show that the rod-shape TiO<sub>2</sub> particles with larger average size exhibit a combination of anatase and brookite phase. The viscoelastic properties of three types of EREs under varying strain amplitude and shear frequency were tested. The results indicate that the long rod-shape TiO<sub>2</sub> particles filled EREs shows higher storage modulus  $G'$  and higher relative ER effect within the electric field from 0 to 3 kV/mm. The observations indicate the use of rod-shape TiO<sub>2</sub> particles in the form of brookite phase may help enhance the ER properties of elastomers. The investigation contributes to the designing, preparation, and application of anisotropic ERE.

## KEYWORDS

electrorheological materials, elastomer, storage modulus, rod-shaped TiO<sub>2</sub> particles, relative ER effect

## 1 Introduction

Electrorheological (ER) materials are one kind of smart materials whose viscoelastic properties can be instantaneously and reversibly varied with external electric field (Winslow, 1949; Jordan and Shaw, 1989; Parthasarathy and Klingenberg, 1996; Zhang et al., 2021). Electrorheological fluids (ERFs) are one kind of ER materials, which are usually composed of dielectric particles and non-conducting liquid (Wen et al., 2003; Dong et al., 2022; Liang et al., 2022; Wang et al., 2022). The rheological performance (shear stress, viscosity, etc.) of ERFs can be changed by applied electric field. Even though the ER effect of ERFs is relatively strong, there are still some impediments for which in practical application, such as sedimentation of dielectric particles and leakage of carrier liquid medium (Zhao and Yin, 2002; Dong et al., 2014; Wang et al., 2022). Since Shiga et al., 1993 developed a kind of polymer composite consisting of silicone elastomer and semiconducting particles in 1993 electrorheological elastomers (EREs) began to enter researchers' horizons. As another branch of ER materials, EREs are generally made by dispersing dielectric particles in cross-linked polymers instead of liquids, and the oriented structure of particles formed by electric

field would be locked in the matrix (Liu, 1999; Gao and Zhao, 2004). Owing to the structures of EREs, their viscoelasticity like modulus and damping factor can be reversibly changed by electric field, which makes them have an application prospect in the field of vibration isolation, electro-drive actuators, soft robot, etc. (Biggerstaff and Kosmatka, 2002; Koyanagi et al., 2009).

The response of EREs to electric field stimulation is generally evaluated by relative ER effect (Dong et al., 2016), which is defined by the following Equation 1.

$$\frac{\Delta G'}{G_0'} = \frac{G_E' - G_0'}{G_0'} \quad (1)$$

where  $G_E'$  and  $G_0'$  are the storage modulus with and without applying external electric field, respectively. To improve the important property parameter for application, many efforts have been done on it. Sirivat et al. prepared several kinds of EREs consisting of different inclusions and matrices such as polythiophene/polyisoprene elastomer (Puvanattvattana et al., 2006), PPV/PDMS (Niamlang and Sirivat, 2008), poly(p-phenylene)/AR71 (Kunanuruksapong and Sirivat, 2007), thermoplastic elastomer polyurethanes (Petcharoen and Sirivat, 2013). Among the above EREs, the maximum relative ER effect could reach 110% at 2 kV/mm. Dong et al. synthesized a kind of ERE by dispersing urea-coated titanium dioxide particles in silicon rubber, the relative ER effects of which could achieve 266% at 3 kV/mm (Niu et al., 2015). Kossi et al. developed a TiO<sub>2</sub>-Acac/PDMS ERE with a maximum storage modulus variation range ( $\Delta G' = G_E' - G_0'$ ) exceeding 500 kPa at 2 kV/mm (Kossi et al., 2015). Wu et al. recently investigated a kind of ERE filled with urea-coated barium titanyl oxalate nanoparticles, which could attain a maximum relative ER effect of 3280% (Yuan et al., 2020).

As a type of composite material that can respond to external stimuli, the properties of dispersed phase particles in ER materials have a significant impact on their ER activity. There have been some research reports on the influence of particle morphology on the rheological properties of elastomers. Liu et al. used numerical techniques to study the effect of particle shape on properties of EREs, and they found the long, thin particles may exhibit higher ER activity than spherical particles (Bo et al., 1999). Gao et al., 2019 prepared spherical, urchin-like, pit-like Mg-doped BaTiO<sub>3</sub> particles filled gelatin hydrogel elastomers, and the results indicated the shape of particles played important roles on electro responsive properties of the elastomers. For ERFs, some studies have focused on the effects of spherical and rod-like particles on ER activity. Kanu and Shaw analyzed the relationship between the shear modulus of ERFs dispersed with spherical and ellipsoidal particles and the geometry of the particles based on electrostatic polarization model, and they got the conclusion that the dielectric properties of ERFs can be enhanced, leading to increased strength of the interactions between adjacent particles (Kanu and Shaw, 1998). By varying the geometric aspect ratio of dispersing particles, Jang et al. found the shear stress of titania-coated silica nanomaterials-based ERFs increases with increasing the aspect ratio (Hong et al., 2010). They also fabricated mesoporous silica particle-based ERFs, and proved the ER performance of that improved with an increasing aspect ratio due to the better flow resistance and mechanical stability (Noh et al., 2016; Yoon et al., 2016; Yoon et al., 2017). Although the above studies on ERFs have proved the influence of dielectric

particle morphology on the ER effect, due to the significant difference in matrix properties between ERF and ERE, the influence of rod-like anisotropic particles on ERE properties need to be further studied.

In this study, spheroid, short rod, and long rod TiO<sub>2</sub> particles were prepared with sol-gel method and used as dispersed phase particles to fill the silicon rubber matrix. The morphology and composition of the elastomers were characterized. Then the dynamic viscoelastic properties of three kinds of EREs were analyzed with a rotational rheometer. Correspondingly, the relationship between the particle morphology and ER performance of the elastomers were further discussed according to the test results.

## 2 Materials and methods

### 2.1 Materials

Triethanolamine (TEOA: N(CH<sub>2</sub>CH<sub>2</sub>OH)<sub>3</sub>, AP) and ethanol (C<sub>2</sub>H<sub>5</sub>OH, AP) were purchased from Tianjin Fuyu Fine Chemical Co., Ltd. Titanium (IV) isopropoxide (TIPO: Ti(OCH(CH<sub>3</sub>)<sub>2</sub>)<sub>4</sub>, AP) was provided by Aladdin Industry Co., Ltd. Diethylenetriamine (DETA: NH<sub>2</sub>CH<sub>2</sub>CH<sub>2</sub>NHCH<sub>2</sub>CH<sub>2</sub>NH<sub>2</sub>, AP) was obtained from Tianjin Guangfu Fine Chemical Research Institute. HClO<sub>4</sub> and NaOH were supplied by Tianjin Kemiou Chemical Reagent Co., Ltd. Silicon RTV 302 and catalyst were purchased from Zhuhai COCA New Materials Co., Ltd. Dimethyl silicon oil ( $\eta = 100$  mPa s, 25°C) was supplied by Beijing Hangping silicon and chemical Co., Ltd. Deionized water was made in the laboratory and used during all experiments. All chemicals were used as received without further purification.

### 2.2 Synthesis of particles

The TiO<sub>2</sub> particles used in this study were all fabricated with sol-gel method. Typical preparation process of spheroid or rod particles is as follows: First, 22.72 g TIPO was mixed with 23.84 g TEOA and vigorously stirred for 10 min to form a compound of Ti<sup>4+</sup> stable against hydrolysis at room temperature. Subsequently, 160 mL deionized water was added to the compound of TIPO and TEOA, and kept stirring for another 30 min to get solution A. Then, a certain amount of DETA was added to 160 mL deionized water and evenly mixed to obtain solution B. The amount of DETA required to prepare the long rod particles was 0.1 mol/L, while DETA is not added when preparing spheroid and short rod particles. Next, according to the different morphology of the prepared particles, HClO<sub>4</sub> or NaOH solution was used to adjust the pH of solution B to different levels to get solution C. For preparing spheroid, short rod and long rod TiO<sub>2</sub> particles, the final pH of solution C should be adjusted to 9.5, 11.2, and 11.35, respectively. After that, solution C was poured into solution A and the mixture was stirred for 15 min. Subsequently, the mixture was transferred into Teflon-lined stainless-steel autoclave, sealed, and maintained at 100°C for 24 h for gelation. Then, the resulting highly viscous gel was aged at 140°C for 3 days to nucleate and grow titania particles (the second aging). In the end, the final products were centrifuged,

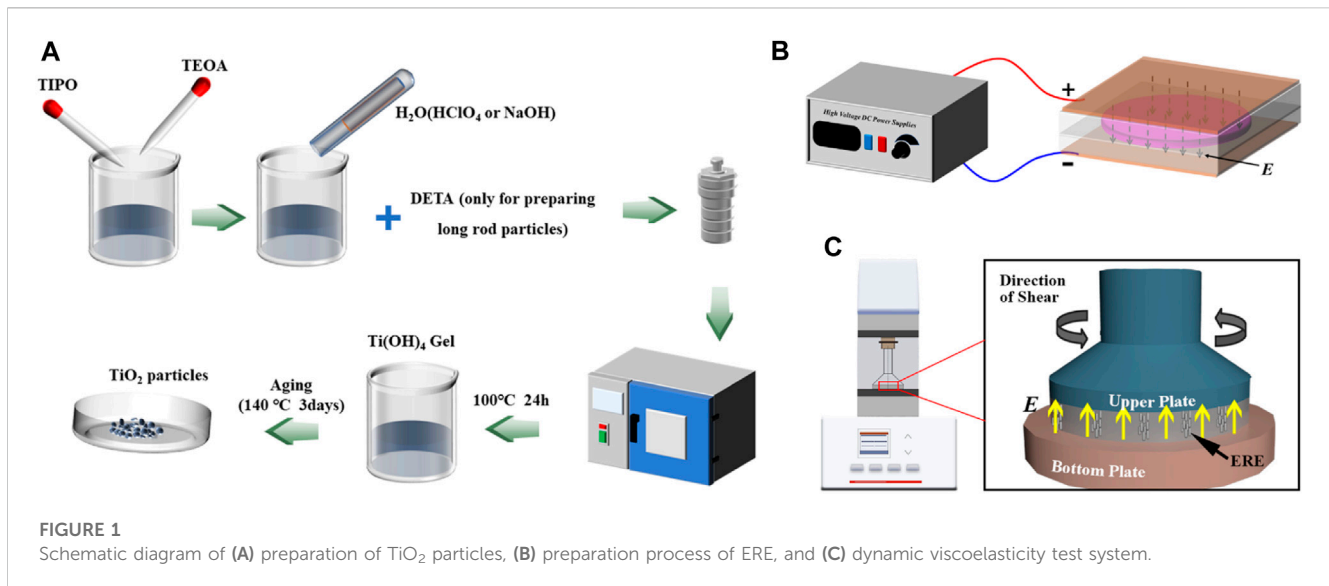


**FIGURE 1**  
Schematic diagram of (A) preparation of TiO<sub>2</sub> particles, (B) preparation process of ERE, and (C) dynamic viscoelasticity test system.

washed with ethanol several times and dried at 60°C for 48 h in a vacuum. The TiO<sub>2</sub> particles were obtained after mechanical grinding of the dried final products. The preparation process of the particles is shown as Figure 1A.

## 2.3 Preparation of EREs

ERE specimens with 35% by weight of different particles were prepared. Silicon RTV 302 and silicon oil with the same weight were mixed and stirred for 15 min. The different TiO<sub>2</sub> particles with a weight fraction of 35% were subsequently added into the rubber mixture, ground, and stirred mechanically for 1 h. Then, the curing agent that accounted for 4% of the weight of silicon RTV was added into the mixture. After the mixture was stirred for another 10 min, it was transferred into a vacuum case to remove the residual bubbles. Finally, the mixture was filled into a mold with a uniform 1 kV/mm electric field applying to both sides of that. After curing for 24 h under the electric field, the anisotropic EREs filled with different TiO<sub>2</sub> particles were obtained. The preparation process of the ERE samples is shown in Figure 1B.

## 2.4 Characterization

The morphology of the particles was observed by a field-emission scanning electron microscope (FSEM) (FEI NOVA NanoSEM 450) with an applied voltage of 3 kV at a work distance of 5 mm and a transmission electron microscope (TEM) (FEI Tecnai F30). An X-ray diffractometer (XRD) (Empyrean) was used to analyze the crystal structure of particles. The average size of particles was measured with Nano Measurer (Malvern Nano-ZS90). Fourier transform infrared (FT-IR) (Nicolet 6700) spectra were employed to determine the chemical structure with a KBr disk method. The dielectric spectra of EREs were examined by a LCR meter (HIOKI IM3536).

The viscoelastic property measurements of different EREs were conducted using a rotational rheometer (Physica MCR 301, Anton

Paar) in which a parallel plate system (PP15-E) was equipped. The diagram of this test system is shown as Figure 1C. The dependence of the storage modulus  $G'$  and loss modulus  $G''$  on strain amplitude with a constant oscillation shear frequency of 10 Hz and an electric field strength of 0, 1, 2, 3 kV/mm were obtained for all ERE specimens. The oscillation shear frequency influence on  $G'$  and  $G''$  was measured at fixed strain amplitude of 0.01% and electric field strength, and the frequency  $f$  was varied in the range of 0.1–100 Hz.

## 3 Results and discussion

### 3.1 Microstructure characterization

SEM images depicting these three kinds of particles that prepared in the experiments are presented in Figure 2. Specifically, in the absence of DETA during particle preparation and when the pH of the solution was maintained at 9.50, the resulting particles exhibited a nearly spheroidal morphology, displaying homogeneity and exceptional dispersion in both size and shape, as shown in Figure 2A. When the pH of the solution was increased to 11.20 without changing the amount of DETA, the morphology of the prepared particles was in the form of short rods and the particles were well dispersed (Figure 2B). Based on the research of Sugimoto et al. (Sugimoto et al., 2003), DETA has a stronger adsorption onto the crystal faces parallel to the  $c$ -axis than  $c$ -faces of TiO<sub>2</sub> in the alkaline range, the shape of rod TiO<sub>2</sub> particles can be further controlled by DETA as a result. If 0.1 mol/L DETA is added to the mixed solution for preparing the particles, and simultaneously adjusting the pH to 11.35, the resulting morphology of the prepared particles is displayed in Figure 2C. As depicted in the figure, it becomes evident that this kind of particle exhibits an overall size augmentation in comparison to the prior short rod-shaped particles. However, it is noteworthy that the size uniformity and dispersion of these particles have noticeably worsened.

Figure 3 shows the TEM images of three kinds of particles with distinct morphologies. The figure clearly depicts a progression in particle size, transitioning from spheroid particles (depicted in

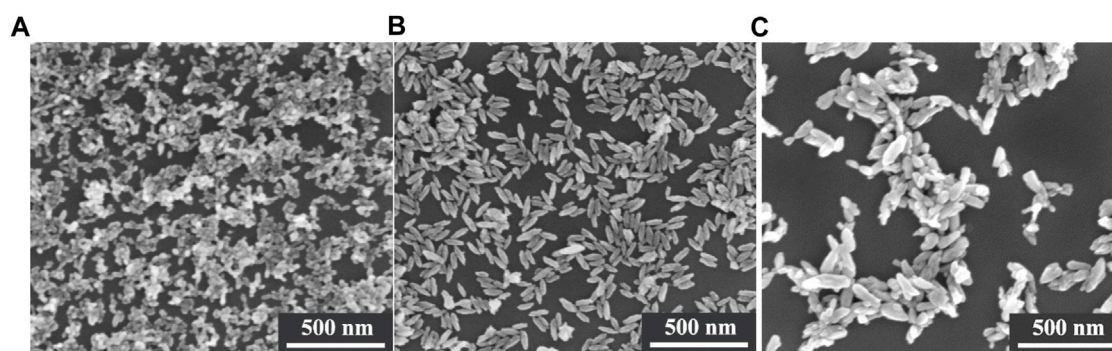


FIGURE 2 SEM images of (A) spheroid, (B) short rod and (C) long rod  $\text{TiO}_2$  particles.

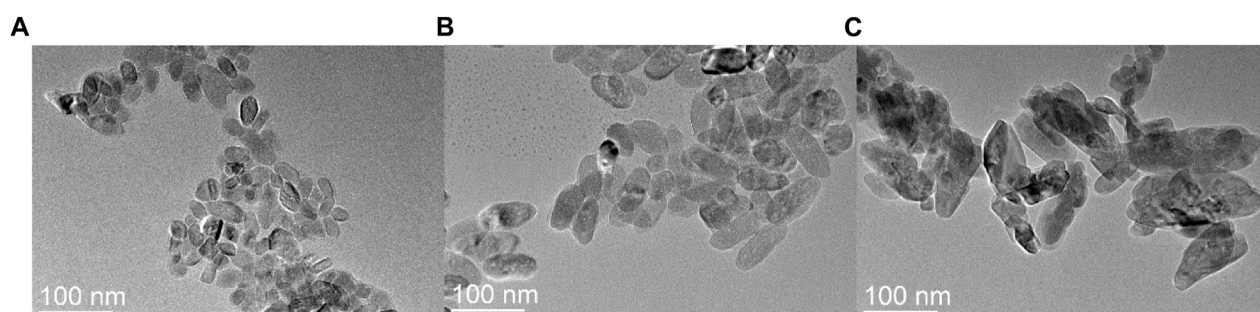


FIGURE 3 TEM micrographs of (A) spheroid, (B) short rod and (C) long rod  $\text{TiO}_2$  particles.

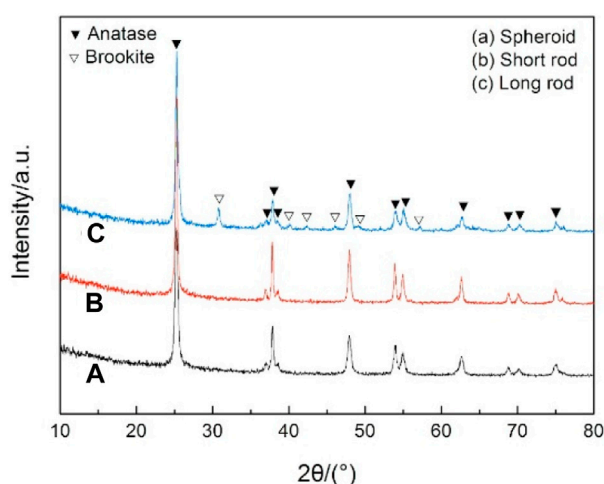


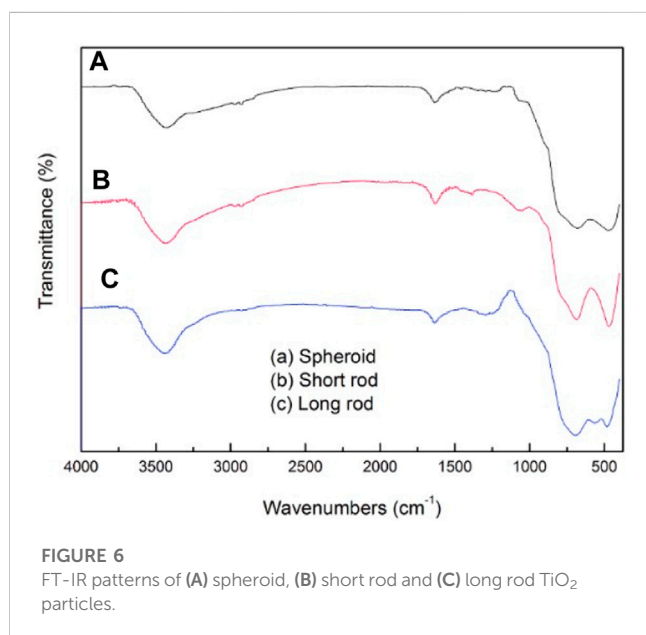
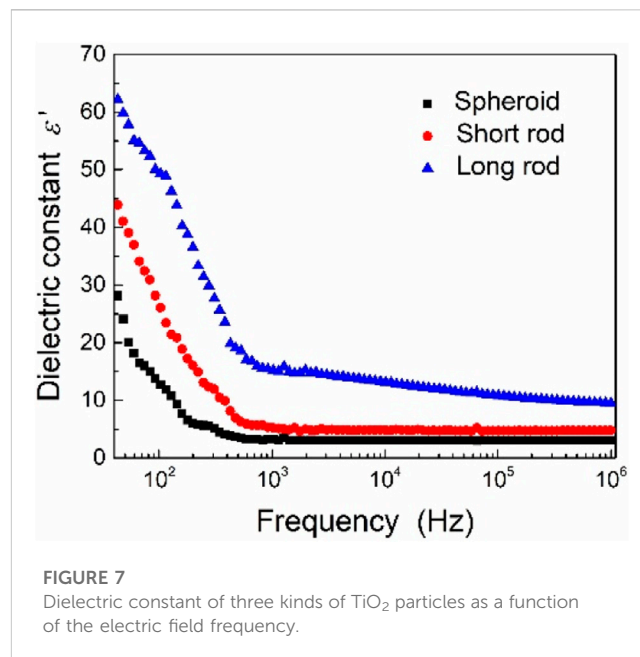
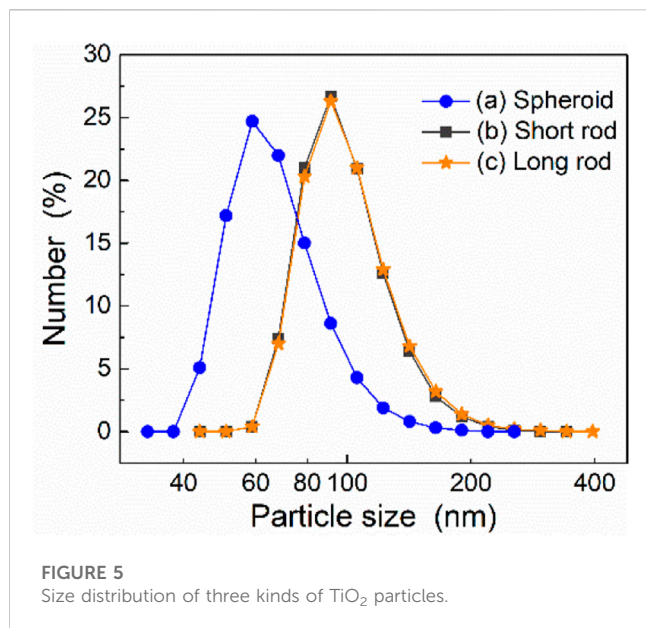
FIGURE 4 XRD patterns of (A) spheroid, (B) short rod and (C) long rod  $\text{TiO}_2$  particles.

Figure 3A) to elongated rod-like structures (observed in Figure 3C). When the particle morphology assumes spheroid or short rod-like shapes, the sample demonstrates a uniform dispersion, resembling a

monodisperse system. Analysis of the data presented in Figure 3A reveals an average diameter of approximately 30 nm for the spherical particles. Figure 3B showcases the short-axis length of the short-rod particles to be around 40 nm, whereas the long axis measures approximately 130 nm, resulting in a length-to-diameter ratio close to 3.25. Figure 3C provides evidence that when the particulate morphology adopts a long rod-like configuration, the particle length increases slightly compared to that of the short rod particles. Although the samples experience slight agglomeration, the particles exhibit well-dispersed characteristics. It is worth noting, however, that some degree of agglomeration occurs, leading to non-uniform morphology and size distribution. Along the long-axis direction, the particles exhibit a length of approximately 145 nm.

The XRD patterns of the prepared three kinds of particles are shown in Figure 4. It can be observed that the anatase crystalline peaks are solely present for both the spherical and short rod-shaped  $\text{TiO}_2$  particles in the diffraction angle range of  $10^\circ$ – $80^\circ$ . This indicates that these two particles are pure anatase phase  $\text{TiO}_2$  with good crystallinity. However, the long rod-shaped  $\text{TiO}_2$  particles exhibit not only the anatase but also the brookite phase of  $\text{TiO}_2$ . Evidently, the aforementioned results suggest that the long rod-shaped  $\text{TiO}_2$  particles produced under these conditions exhibit a combination of the anatase and brookite phase of  $\text{TiO}_2$ .

Figure 5 shows the size distribution of these three types of particles. The analysis results unveil average diameters of the



spheroid, short rod-shaped, and long rod-shaped particles are 108.1 nm, 133.4 nm, and 143.7 nm, respectively. Comparing with the aforementioned TEM analysis results, the particle size analysis values of short rod-shaped and long rod-shaped particles are close to them, while the analytical values of spheroid particles in Figure 5 are much larger. This can be attributed to two possible factors: One is the smaller size of the nanoscale spherical particles can induce agglomeration, while that might be recognized by Nano Measurer as particles with larger size; the other one might be attributed to the absorption of organics or particle debris onto the particle surface during the preparation of the samples for particle size analysis. Nevertheless, the results obtained from the particle size analysis hold greater statistical significance. The particle size analysis can help us to understand the average particle size of a large number of particles,

whereby the variation of particle size among the three samples can be effectively confirmed. In addition, Due to the agglomeration of nanoscale particles, the particle size of short rod-shaped particles is not significantly different from that of long rod-shaped particles, as shown in Figure 5. However, it can still be found from this figure that compared to short rod-shaped particles, long rod-shaped particles have a higher number of larger particle sizes, while smaller particle sizes are fewer, which indicates that the average size of long rod particles is larger in the long-axis direction.

The infrared spectra of three kinds of TiO<sub>2</sub> particles with different morphologies are shown in Figure 6. In the spheroid particles shown in spectral line (a), the band around 3425.54 cm<sup>-1</sup> originates from the stretching vibration of the hydrogen bond O-H. The band at 1632.57 cm<sup>-1</sup> correspond to the superposition of the H-O-H and C=N stretching vibration. The vibrational peaks at 674.84 cm<sup>-1</sup> and 427.63 cm<sup>-1</sup> originate from the stretching vibration of the Ti-O bond. The infrared spectra of short rod-shaped particles is shown as spectral line (b), the peak at 3429.02 cm<sup>-1</sup> is assigned to the stretching vibration of the hydrogen bond O-H, the superposition of the H-O-H and C=N stretching vibrational peaks occurs at 1632.07 cm<sup>-1</sup>. Besides, the vibrational peaks at 685.67 cm<sup>-1</sup> and 467.29 cm<sup>-1</sup> both stand for the stretching vibrations of the Ti-O bond. In the spectra of long rod-shaped particles (Figure 6C), the vibrational peak at 3442.21 cm<sup>-1</sup> is attributed to the stretching vibration of O-H, and the superposition of the H-O-H and C=N stretching vibrational peaks occurs at 1633.76 cm<sup>-1</sup>. The vibrational peaks at 692.15 cm<sup>-1</sup> and 482.84 cm<sup>-1</sup> both correspond to the Ti-O vibration. From the results of the infrared absorption peaks, it can be seen that these three kinds of particles are all TiO<sub>2</sub> particles with hydroxyl groups on the surface.

### 3.2 Characterization of elastomers

The dependence of dielectric constant on electric field frequency for the elastomers filled with three kinds of TiO<sub>2</sub> particles is

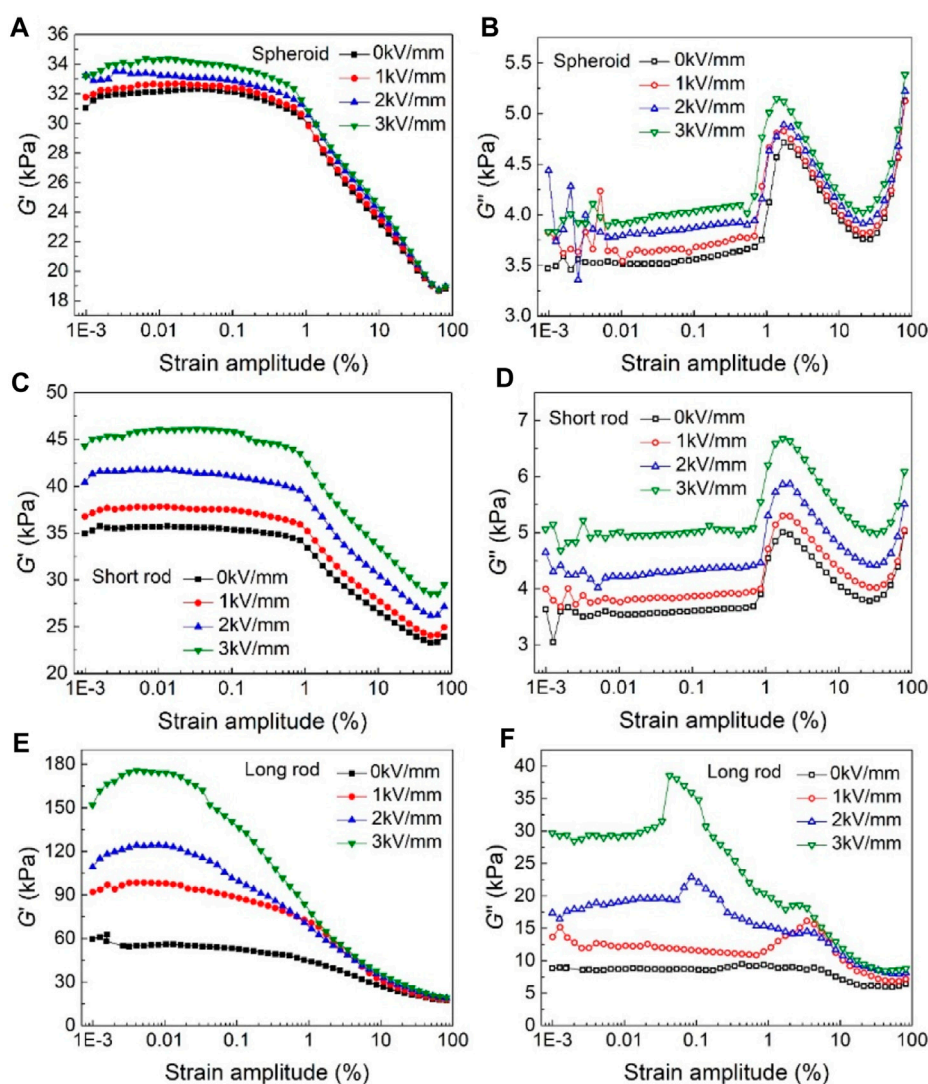


FIGURE 8

Storage modulus  $G'$  and loss modulus  $G''$  of EREs filled with spheroid (A, B), short rod (C, D) and long rod (E, F)  $\text{TiO}_2$  particles as a function of strain amplitude.

presented in Figure 7. It is clearly found that the dielectric constants are obviously enhanced for the elastomers containing rod-shaped particles with respect to that filled with spheroid  $\text{TiO}_2$  particles. Moreover, the ERE filled with long rod-shaped  $\text{TiO}_2$  particles shows the highest dielectric constant among these three kinds of samples, which may be attributed to the stronger dipolar polarization of brookite phase of  $\text{TiO}_2$  with long rod shape.

The storage modulus  $G'$  and loss modulus  $G''$  of EREs filled with spheroid, short rod, and long rod  $\text{TiO}_2$  particles as a function of strain amplitude are shown in Figure 8. Comparing Figures 8A,C,E, the storage modulus  $G'$  of elastomers filled with spheroid and short rod-shaped particles are close to each other under zero-field, while the  $G'$  of long rod-shaped particles filled EREs is larger. Due to the good dielectric properties of long rod-shaped particles, they can help form a stronger columnar particle-oriented structures under the rubber curing electric field. This structure will have a stronger hindrance to the movement of rubber molecular chain segments, resulting in a

higher energy storage modulus of the elastomer containing long rod-shaped particles under zero field. Meanwhile, it can be seen from these three figures that when the electric field strength increases from 0 kV/mm to 3 kV/mm,  $G'$  of EREs filled with spheroid particles does not change significantly, while that of the EREs filled with short rod and long rod-shaped  $\text{TiO}_2$  particles have a small and a significant increase with the increasing electric field strength, respectively. In addition, except for the EREs filled with long rod-shaped particles at a field strength of 3 kV/mm, the  $G'$  of the other two kinds of EREs show almost no change in the range of 0%–1%, which is defined as the linear viscoelastic (LVE) range (Figures 8A,C,E). With the increase of shear strain, the  $G'$  values of the EREs all start to decrease and then enters the nonlinear region, which can be attributed to the destruction of the chain or fiber like structures formed by the filled particles inside the EREs. This phenomenon is called the Payne effect of the EREs.

As shown in Figures 8B,D,F, the loss modulus  $G''$  versus strain variation curves of elastomers filled with three kinds of  $\text{TiO}_2$  particles. It

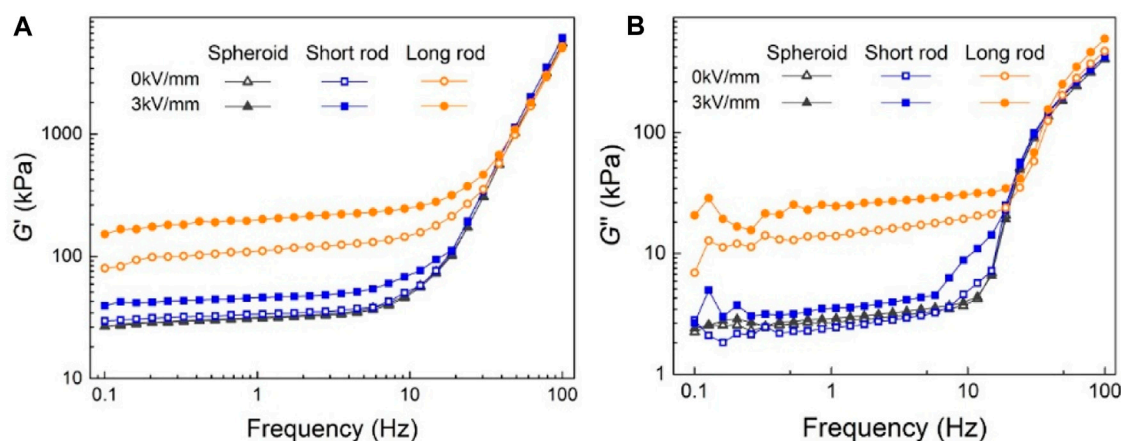


**FIGURE 9** Storage modulus  $G'$  (A) and loss modulus  $G''$  (B) of EREs filled with spheroid, short rod, and long rod  $\text{TiO}_2$  particles as a function of oscillation shear frequency.

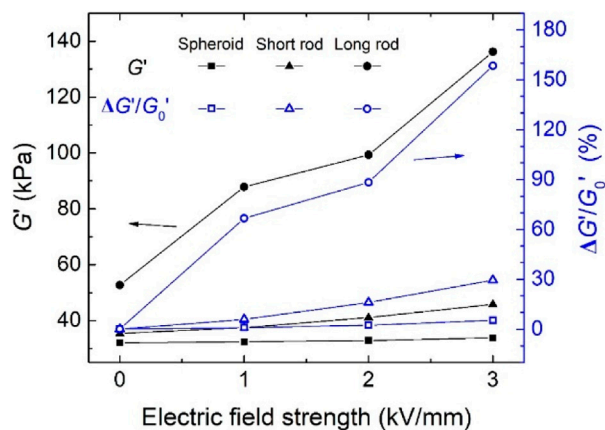


**FIGURE 10** Tunable range of storage modulus  $G'$  and relative ER effect of EREs filled with spheroid, short rod, and long rod  $\text{TiO}_2$  particles.

can be seen from these figures that the loss modulus  $G''$  increases slowly with the increasing shear strain at different field strengths in the LVE range. However, when the strain amplitude is further increases by more than 1%, that is, beyond the range of LVE range, the  $G''$  starts to decrease owing to the friction between the chain structure and the elastomer matrix is weakened, which is also mainly attributed to the damage of the particle chain structures in the EREs under stress. Afterwards, as the shear strain amplitude continues to increase, the  $G''$  of the three types of EREs show an increasing trend. This may be due to the increased friction between the molecular chains within the elastomer matrix at this stage, which contributes to the  $G''$  of elastomer.

The storage modulus  $G'$  and loss modulus  $G''$  of EREs filled with spheroid, short rod, and long rod  $\text{TiO}_2$  particles as a function of oscillation shear frequency are shown in Figure 9. As can be seen in Figures 9A,B, when the shear frequency is varied in the range of 0–10 Hz, the  $G'$  and  $G''$  of each elastomer do not change, indicating that they are in the LVE range. When the shear frequency exceeds 10 Hz, the chain segments in the elastomer cannot undergo

orientation movement in time due to the applied high-frequency shear stress, and the elastomer exhibits rigidity. At this time, the shear storage modulus  $G'$  increases. Besides, the loss modulus  $G''$  of each ERE also increases substantially due to the increased friction between the molecular chains within the matrix and between the molecular chains and the filler particle chains under high-frequency shear.

The variation curves of the storage modulus  $G'$  and relative ER effect of EREs with the applied electric field strength are shown in Figure 10. As can be seen from this figure, when the applied electric field strength is increased from 0 kV/mm to 3 kV/mm, the changes in the  $G'$  of the spheroid and short rod-shaped particles filled EREs are small. Besides, the relative ER effects of EREs containing spheroid and short rod-shaped particles are 5.3% and 29.4% at 3 kV/mm, respectively. Whereas, the storage modulus  $G'$  of the EREs filled with long rod-shaped  $\text{TiO}_2$  particles at a field strength of 3 kV/mm reaches 136.2 kPa, and the relative ER effect can reach 158.4%.

## 4 Conclusion

$\text{TiO}_2$  particles with spherical, short rod, and long rod morphology were synthesized by sol-gel method, and the morphologies of different particles were confirmed by SEM and TEM results. XRD analysis indicated the spheroid and short rod-shaped particles were pure anatase phase  $\text{TiO}_2$ , while the long rod-shaped  $\text{TiO}_2$  particles exhibit a combination of the anatase and brookite phase of  $\text{TiO}_2$ . Three kinds of EREs were prepared by dispersing these different types of particles in a silicon rubber matrix. Owing to the improved polarizability of long rod-shaped  $\text{TiO}_2$  of brookite phase, the elastomer containing long rod  $\text{TiO}_2$  presents larger dielectric constant, indicating better ER activity. Since the movement of rubber chains is restrained by the stronger particle chain structures formed by long rod-shaped  $\text{TiO}_2$ , the storage modulus  $G'$  of EREs filled with long rod-shaped  $\text{TiO}_2$  particles under zero-field is larger than the other two kinds of EREs. Moreover, the dynamic viscoelastic test also illustrates that the EREs containing long rod-shaped  $\text{TiO}_2$  particles have high performance in terms of field-induced storage modulus

and relative ER effect in the electric field range of 0–3 kV/mm. The enhanced ER activity possibly benefit from the stronger polarization of long rod-shaped TiO<sub>2</sub> particles and columnar particle-oriented structures in the elastomer matrix.

## Data availability statement

The raw data supporting the conclusion of this article will be made available by the authors, without undue reservation.

## Author contributions

GT: Methodology, Writing—original draft. YF: Visualization, Writing—review and editing. JT: Formal Analysis, Writing—review and editing. CN: Conceptualization, Supervision, Writing—review and editing. XX: Validation, Writing—review and editing.

## Funding

The author(s) declare financial support was received for the research, authorship, and/or publication of this article. This research

## References

- Biggerstaff, J. M., and Kosmatka, J. B. (2002). “Smart structures and materials 2002: electroactive polymer actuators and devices,” in *Bellingham: spie-int soc optical engineering*. Editor Y. BarCohen (Bellingham, Washington: SPIE), 345–350.
- Bo, L., Boggs, S. A., and Shaw, M. T. (1999). “Numerical simulation of electrorheological properties of anisotropically filled elastomers,” in 1999 Annual Report Conference on Electrical Insulation and Dielectric Phenomena (Cat. No.99CH36319), Austin, TX, USA, 17–20 October 1999 (IEEE), 82–85.
- Dong, X. F., Niu, C. G., and Qi, M. (2016). Enhancement of electrorheological performance of electrorheological elastomers by improving TiO<sub>2</sub> particles/silicon rubber interface. *J. Mater. Chem. C* 4 (28), 6806–6815. doi:10.1039/c6tc01447j
- Dong, Y., Yin, J., and Zhao, X. (2014). Microwave-synthesized poly(ionic liquid) particles: a new material with high electrorheological activity. *J. Mater. Chem. A* 2 (25), 9812–9819. doi:10.1039/c4ta00828f
- Dong, Y., Zhao, X., Peng, C., Zhao, R., Zhang, Y., Zhao, P., et al. (2022). Enhanced electrorheological effectiveness and temperature effect of suspensions based on poly(ionic liquid)s neutralized with mixed counterions. *Polymer* 255, 125152. doi:10.1016/j.polymer.2022.125152
- Gao, L., Zhan, L., Liu, W., Zhang, Y., Xie, Z., and Ren, J. (2019). Preparation and electro responsive properties of Mg-doped BaTiO<sub>3</sub> with novel morphologies. *J. Mater. Science-Materials Electron.* 30 (13), 12107–12112. doi:10.1007/s10854-019-01568-7
- Gao, L. X., and Zhao, X. P. (2004). Electrorheological behaviors of barium titanate/gelatin composite hydrogel elastomers. *J. Appl. Polym. Sci.* 94 (6), 2517–2521. doi:10.1002/app.21212
- Hong, J. Y., Choi, M., Kim, C., and Jang, J. (2010). Geometrical study of electrorheological activity with shape-controlled titania-coated silica nanomaterials. *J. Colloid Interface Sci.* 347 (2), 177–182. doi:10.1016/j.jcis.2010.03.054
- Jordan, T. C., and Shaw, M. T. (1989). Electrorheology. *Ieee Trans. Electr. Insulation* 24 (5), 849–878. doi:10.1109/14.42162
- Kanu, R. C., and Shaw, M. T. (1998). Enhanced electrorheological fluids using anisotropic particles. *J. Rheology* 42 (3), 657–670. doi:10.1122/1.550944
- Kossi, A., Bossis, G., and Persello, J. (2015). Electro-active elastomer composites based on doped titanium dioxide. *J. Mater. Chem. C* 3 (7), 1546–1556. doi:10.1039/c4tc02535k
- Koyanagi, K., Yamaguchi, T., Kakinuma, Y., Anzai, H., Sakurai, K., and Oshima, T. (2009). Basic research of electro-rheological gel drum for novel linear actuator. *J. Phys. Conf. Ser.* 149 (1), 012020. doi:10.1088/1742-6596/149/1/012020
- Kunanurksapong, R., and Sirivat, A. (2007). Poly(p-phenylene) and acrylic elastomer blends for electroactive application. *Mater. Sci. Eng. a-Structural Mater. Prop. Microstruct. Process.* 454, 453–460. doi:10.1016/j.msea.2006.12.033
- Li, Y., Liu, Y., Zhou, Y., Shi, Q., Zhang, M., Li, Y., et al. (2022). Efficient and stable electrorheological fluids based on chestnut-like cobalt hydroxide coupled with surface-functionalized carbon dots (Apr, 10.1039/D2SM00176D, 2022). *Soft Matter* 18 (20), 4031. doi:10.1039/d2sm90062a
- Liu, B. (1999). Study of the electrorheology of filled silicone elastomers. *Abstr. Pap. Am. Chem. Soc.* 218, U619–U620.
- Niamlang, S., and Sirivat, A. (2008). Dielectrophoresis force and deflection of electroactive poly(p-phenylene vinylene)/polydimethylsiloxane blends. *Smart Mater. Struct.* 17 (3), 035036. doi:10.1088/0964-1726/17/3/035036
- Niu, C. G., Dong, X. F., and Qi, M. (2015). Enhanced electrorheological properties of elastomers containing TiO<sub>2</sub>/urea core-shell particles. *ACS Appl. Mater. Interfaces* 7 (44), 24855–24863. doi:10.1021/acsami.5b08127
- Noh, J., Yoon, C. M., and Jang, J. (2016). Enhanced electrorheological activity of polyaniline coated mesoporous silica with high aspect ratio. *J. Colloid Interface Sci.* 470, 237–244. doi:10.1016/j.jcis.2016.02.061
- Parthasarathy, M., and Klingenberg, D. J. (1996). Electrorheology: mechanisms and models. *Mater. Sci. Eng. R-Reports* 17 (2), 57–103. doi:10.1016/0927-796x(96)00191-x
- Petcharoen, K., and Sirivat, A. (2013). Electrostrictive properties of thermoplastic polyurethane elastomer: effects of urethane type and soft-hard segment composition. *Curr. Appl. Phys.* 13 (6), 1119–1127. doi:10.1016/j.cap.2013.03.005
- Puvanattana, T., Chotpattananont, D., Hiamtup, P., Niamlang, S., Sirivat, A., and Jamieson, A. M. (2006). Electric field induced stress moduli in polythiophene/polyisoprene elastomer blends. *React. Funct. Polym.* 66 (12), 1575–1588. doi:10.1016/j.reactfunctpolym.2006.06.001
- Shiga, T., Okada, A., and Kurauchi, T. (1993). Electroviscoelastic effect of polymer blends consisting of silicone elastomer and semiconducting polymer particles. *Macromolecules* 26 (25), 6958–6963. doi:10.1021/ma00077a038
- Sugimoto, T., Zhou, X. P., and Muramatsu, A. (2003). Synthesis of uniform anatase TiO<sub>2</sub> nanoparticles by gel-sol method 4. Shape control. *J. Colloid Interface Sci.* 259 (1), 53–61. doi:10.1016/s0021-9797(03)00035-3
- Wang, Y. D., Yuan, J. H., Zhao, X. P., and Yin, J. B. (2022). Electrorheological fluids of GO/Graphene-Based nanoplates. *Materials* 15 (1), 311. doi:10.3390/ma15010311
- Wen, W. J., Huang, X. X., Yang, S. H., Lu, K. Q., and Sheng, P. (2003). The giant electrorheological effect in suspensions of nanoparticles. *Nat. Mater.* 2 (11), 727–730. doi:10.1038/nmat993
- Winslow, W. M. (1949). Induced fibrillation of suspensions. *J. Appl. Phys.* 20 (12), 1137–1140. doi:10.1063/1.1698285

Yoon, C. M., Lee, K., Noh, J., Lee, S., and Jang, J. (2016). Electrorheological performance of multigram-scale mesoporous silica particles with different aspect ratios. *J. Mater. Chem. C* 4 (8), 1713–1719. doi:10.1039/c5tc04124d

Yoon, C. M., Noh, J., Jang, Y., and Jang, J. (2017). Fabrication of a silica/titania hollow nanorod and its electroresponsive activity. *Rsc Adv.* 7 (32), 19754–19763. doi:10.1039/c7ra01786c

Yuan, X., Zhou, X., Liang, Y., Wang, L., Chen, R., Zhang, M., et al. (2020). A stable high-performance isotropic electrorheological elastomer towards controllable and

reversible circular motion. *Compos. Part B Eng.* 193, 107988. doi:10.1016/j.compositesb.2020.107988

Zhang, G., Zhao, X., Jin, X., Zhao, Z., Ren, Y., Wang, L. M., et al. (2021). Ionic-liquid-modified TiO<sub>2</sub> spheres and their enhanced electrorheological responses. *J. Mol. Liq.* 338, 116696. doi:10.1016/j.molliq.2021.116696

Zhao, X. P., and Yin, J. B. (2002). Preparation and electrorheological characteristics of rare-earth-doped TiO<sub>2</sub> suspensions. *Chem. Mater.* 14 (5), 2258–2263. doi:10.1021/cm011522w